Experimental and Theoretical Studies of Sodium Cation Complexes of the Deamidation and Dehydration Products of Asparagine, Glutamine, Aspartic Acid, and Glutamic Acid

A. L. Heaton, S. J. Ye, and P. B. Armentrout*

Department of Chemistry, University of Utah, Salt Lake City, Utah 84112

Received: January 16, 2008

The deamidation and dehydration products of $Na^+(L)$, where L = asparagine (Asn), glutamine (Gln), aspartic acid (Asp), and glutamic acid (Glu), are examined in detail utilizing collision-induced dissociation (CID) with Xe in a guided ion beam tandem mass spectrometer (GIBMS). Results establish that the $Na^+(L)$ complexes decompose upon formation in our dc discharge/flow tube ion source to form a bis-ligand complex, $Na^+(L-HX)(HX)$, composed of a sodium cation, the (L−HX) decomposition product, and HX, where HX = NH_3 for the amides and H_2O for the acids. Analysis of the energy-dependent CID cross sections for the $Na^+(L-HX)(HX)$ complexes provides unambiguous identification of the (L−HX) fragmentation products as 3-amino succinic anhydride (a-SA) for Asx and oxo-proline (O-Pro) for Glx. Furthermore, these experiments establish the 0 K sodium cation affinities for these five-membered ring decomposition products and the H_2O and NH_3 binding affinities of the Na^+(a-SA) and Na^+(O-Pro) complexes after accounting for unimolecular decay rates, the internal energy of reactant ions, and multiple ion−molecule collisions. Quantum chemical calculations are determined for a number of geometric conformations of all reaction species as well as a number of candidate species for (L−HX) at the B3LYP/6-311+G(d,p) level with single-point energies calculated at MP2(full), B3LYP, and B3P86 levels using a 6-311+G(2d,2p) basis set. This coordinated examination of both the experimental work and quantum chemical calculations allows for a complete characterization of the products of deamidation and dehydration of Asx and Glx, as well as the details of Na^+, H_2O, and NH_3 binding to the decomposition species.

Introduction

The deamidation of asparagine (Asn) and glutamine (Gln) residues from the terminal carboxamide functional group in their side chains is the most common type of spontaneous post-translational modification that occurs in proteins. This reaction has been linked to the process of biological aging[1,2] as well as a number of degenerative diseases.[3−8] Similar dehydration reactions of aspartic acid (Asp) and glutamic acid (Glu) at the terminal carboxylic acid functional group in their side chains are also significant biologically, and these reactions likely proceed via comparable mechanisms. Therefore, a molecular characterization of the products of Asx and Glx deamidation and dehydration correlated to these biological processes should prove insightful. Furthermore, a detailed understanding of the molecular interactions of these products with small biologically relevant entities (Na^+, NH_3, and H_2O) may afford quantitative insight into these degradation reactions.

Studying the Asn, Gln, Asp, and Glu ligands concurrently allows for the structural parallels among these four amino acids to be used in uncovering mechanistic details of the deamidation and dehydration processes. The amides, Asn and Gln, differ from the acids, Asp and Glu, by the difference of a carboxamide and carboxylic acid functional group in their side chains, respectively. Furthermore, the Asx and Glx amino acids differ by having one-carbon and two-carbon linkages preceding this group, respectively. Thus, informative trends related to these structural parallels can be drawn, combined with characterizations of similar systems currently available in the literature.

The products of Asx and Glx deamidation and dehydration have been investigated previously for a number of different systems both in the solution phase and in the gas phase. Capasso et al.[9,10] propose that the biological decomposition of Asx residues proceeds through a five-membered succinic ring intermediate, and consistent gas-phase mechanisms for Asx decomposition have also been proposed.[11] The analogue of this product from the monomeric Asx amino acids is 3-amino succinic anhydride (a-SA). For the Glx amino acids, the products of deamidation and dehydration are less established, although several different schemes for how Glx amino acids lose H_2O and NH_3 have been proposed.[12] Significant biologically is the product oxo-proline (O-Pro), which has been identified as the N-terminal amino acid of a large number of naturally occurring proteins.[13] Furthermore, collision-induced dissociation (CID) studies of the intact $Na^+(L)$ complexes, where L = Asn, Asp, Gln, and Glu, utilizing an electrospray ionization (ESI) source produce minor reaction channels corresponding to H_2O or NH_3 loss from Na^+(Asx) and Na^+(Glx) upon collisional excitation.[14] No direct measurements of Na^+, NH_3, or H_2O binding to the products of Asx and Glx deamidation and dehydration have been accomplished previously.

In the work presented here, we explicitly identify the deamidation and dehydration products of the Na^+(Asx) and Na^+(Glx) complexes by experimentally examining $Na^+(L-HX)(HX)$ complexes, where HX = NH_3 for the amides and H_2O for the acids. Investigation of all possible candidate fragments relevant to these studies is provided at length below and shows that (L−HX) is 3-amino succinic anhydride (a-SA) for Asx and oxo-proline (O-Pro) for Glx. Thus, we are able to

* To whom correspondence should be addressed.

10.1021/jp800439j CCC: $40.75
Published on Web 03/21/2008

provide the first experimental values for the Na^+ binding affinities of a-SA and O-Pro and the H_2O and NH_3 binding affinities of Na^+(a-SA) and Na^+(O-Pro). Absolute bond dissociation energies (BDEs) are measured using threshold CID (TCID) in a guided ion beam tandem mass spectrometer. Theoretical calculations at the B3LYP/6-311+G(d,p) level are carried out to provide structures, vibrational frequencies, and rotational constants needed for analysis of the TCID data. Experimental BDEs are compared to theoretical calculations performed for a number of possible geometries at the B3LYP/6-311+G(2d,2p), B3P86/6-311+G(2d,2p), and MP2(full)/6-311+G(2d,2p) levels using geometries and zero-point energy corrections calculated at the B3LYP/6-311+G(d,p) level of theory along with corrections for basis set superposition errors (BSSE).

Experimental and Computational Section

General Experimental Procedures. Cross sections for CID of the metal−ligand complexes are measured using a guided ion beam tandem mass spectrometer that has been described in detail previously.[15,16] The present studies are conducted using a direct current discharge flow tube (DC/FT) source,[17] under conditions similar to those described previously.[18] Briefly, the DC/FT source generates sodium cations in a 1 m long flow tube via a continuous dc discharge by argon ion sputtering of a cathode made from a tantalum rod with a small cutout containing sodium metal. Typical operating conditions of the discharge are 1.4−2.0 kV and 8−20 mA. The sodium cations produced are carried by a flow of buffer gas of ~10% Ar in He through a 1 m long flow tube at a rate of 500−700 standard cm^3/min each, usually at a pressure of 0.4−0.9 Torr. Neutral ligands (here, the four amino acids) are introduced approximately 50 cm downstream from the discharge via a probe containing the amino acid that is heated to temperatures in the range of 160−210 °C. Complexes are formed by three-body association reactions of the sodium cation with the neutral ligands. The ions undergo multiple collisions ($>10^5$) with the room-temperature flow gases. Thus, the DC/FT source is assumed to produce ions having their internal energies well described by a Maxwell−Boltzmann distribution of rovibrational states at 300 K, as characterized in previous experiments.[17,18,20−24]

Metal−ligand complexes are then extracted from the source and mass selected using a magnetic momentum analyzer. The mass-selected ions are decelerated to a well-defined kinetic energy and are focused into a rf octopole ion guide that traps the ions radially.[25,26] The ion guide minimizes losses of the reactant and any product ions resulting from scattering. The octopole passes through a static gas cell containing xenon, which is used as the collision gas for reasons described elsewhere.[27,28] After collision, the reactant and product ions drift to the end of the octopole where they are extracted and focused into a quadrupole mass filter for mass analysis. The ions are detected with a high-voltage dynode, scintillation ion detector, and the signal is processed using standard pulse counting techniques. Ion intensities, measured as a function of collision energy, are converted to absolute cross sections, as described previously.[15] The uncertainty in relative cross sections is about ±5%, and that for the absolute cross sections is about ±20%. The ion kinetic energy distribution is measured to be Gaussian and has a typical fwhm of ~0.3 eV (lab) for the DC/FT source. Uncertainties in the absolute energy scale are about ±0.05 eV (lab). Ion kinetic energies in the laboratory frame are converted to energies in the center-of-mass (CM) frame using $E_{CM} = E_{lab}m/(m + M)$, where M and m are the masses of the ionic and neutral reactants, respectively. All energies herein are reported in the CM frame unless otherwise noted.

Thermochemical Analysis. Threshold regions of the CID reaction cross sections are modeled using eq 1

$$\sigma_j(E) = (n\sigma_{0,j}/E) \sum g_i \int_{E_{0,j}-E_i}^{E} [k_j(E^*)/k_{tot}(E^*)] \times \{1 - e^{-k_{tot}(E^*)\tau}\}(E - \epsilon)^{n-1} d(\epsilon) \quad (1)$$

where $\sigma_{0,j}$ is an energy-independent scaling factor for channel j, n is an adjustable parameter that describes the efficiency of collisional energy transfer,[16] E is the relative kinetic energy of the reactants, $E_{0,j}$ is the threshold for dissociation of the ground electronic and rovibrational state of the reactant ion at 0 K for channel j, τ is the experimental time for dissociation ($\sim 5 \times 10^{-4}$ s in the extended dual octopole configuration as measured by time-of-flight studies),[16] ϵ is the energy transferred from translation during the collision, and E^* is the internal energy of the energized molecule (EM) after the collision, that is, $E^* = \epsilon + E_i$. The summation is over the rovibrational states of the reactant ions, i, where E_i is the excitation energy of each state and g_i is the fractional population of those states ($\sum g_i = 1$). The Beyer−Swinehart algorithm[29−31] is used to evaluate the number and density of the rovibrational states, and the relative populations g_i are calculated for a Maxwell−Boltzmann distribution at 300 K.

The term $k_j(E^*)$ is the unimolecular rate constant for dissociation of the energized molecule to channel j. The rate constants $k_j(E^*)$ and $k_{tot}(E^*)$ are defined by Rice−Ramsperger−Kassel−Marcus (RRKM) theory as in eq 2[32,33]

$$k_{tot}(E^*) = \sum_j k_j(E^*) = \sum_j d_j N_j^{\dagger}(E^* - E_{0,j})/h\rho(E^*) \quad (2)$$

where d_j is the reaction degeneracy of channel j, $N_j^{\dagger}(E^* - E_{0,j})$ is the sum of rovibrational states of the transition state (TS) for channel j at an energy $E^* - E_{0,j}$, and $\rho(E^*)$ is the density of states of the energized molecule (EM) at the available energy, E^*. These rate constants allow both kinetic shifts and competition between multiple parallel channels to be modeled.[34,35] When no significant competition among product channels is observed, the term $k_j(E^*)/k_{tot}(E^*) = 1$ and all fitting parameters then correspond to the single channel being modeled.

Several effects that obscure the interpretation of the data must be accounted for during data analysis in order to produce accurate thermodynamic information. The first effect involves energy broadening resulting from the thermal motion of the neutral collision gas and the kinetic energy distribution of the reactant ion. This is accounted for by explicitly convoluting the model over both kinetic energy distributions, as described elsewhere in detail.[15] The second effect considers that eq 1 only models cross sections that represent products formed as the result of a single-collision event. To ensure rigorous single-collision conditions, data are collected at three pressures of Xe, generally about 0.16, 0.08, and 0.04 mTorr, and the resulting cross sections are evaluated for pressure effects and extrapolated to zero pressure when necessary.[36] The third effect arises from the lifetime for dissociation. As the size of reactant molecules increases, so do the number of vibrational modes of the reactant ion and thus the time for energy randomization into the reaction coordinate after collision. Thus, some energized molecules may not dissociate during the time scale of the experiment.[34] This leads to a delayed onset for the CID threshold, a kinetic shift, which becomes more noticeable as the size of the molecule increases. These kinetic shifts are estimated by the incorporation

of RRKM theory as shown in eq 1 and as described in detail elsewhere.[34] To evaluate the rate constant in eq 1, sets of rovibrational frequencies for the EM and all TSs are required. Because the metal−ligand interactions in our $Na^+(L-HX)(HX)$ complexes are mainly electrostatic, the most appropriate model for the TS for dissociation of the intact ligand is a loose association of the ion and neutral ligand fragments. The appropriateness of this assumption for multidentate ligands has been verified previously for crown ethers[37,38] and more recently for the tripeptide, GlyGlyGly.[39] Therefore, these TSs are treated as product-like, such that the TS frequencies are those of the dissociation products. The molecular parameters needed for the RRKM calculation are taken from the quantum chemical calculations detailed in the next section. The transitional frequencies in the TSs are treated as rotors, a treatment that corresponds to a phase space limit (PSL), as described in detail elsewhere.[34,35] The 2D external rotations are treated adiabatically but with centrifugal effects included.[31] In the present work, the adiabatic 2D rotational energy is treated using a statistical distribution with an explicit summation over all of the possible values of the rotational quantum number.[34,35]

The model cross sections of eq 1 are convoluted with the kinetic energy distribution of the reactants and compared to the data. A nonlinear least-squares analysis is used to provide optimized values for $\sigma_{0,j}$, n, and $E_{0,j}$. The uncertainty associated with $E_{0,j}$ is estimated from the range of threshold values determined from different data sets with variations in the parameter n, variations in vibrational frequencies (±10% in most frequencies and a factor of 2 for the metal−ligand modes), changes in τ by factors of 2, and the uncertainty of the absolute energy scale, 0.05 eV (lab).

In deriving the final optimized BDEs at 0 K, two assumptions are made. First, we assume that there is no activation barrier in excess of the reaction endothermicity for the loss of ligands, which is generally true for ion−molecule reactions and for the heterolytic noncovalent bond dissociations considered here.[40] Second, the measured threshold E_0 values for dissociation are from ground-state reactant to ground-state ion and neutral ligand products. Given the relatively long experimental time frame ($\sim 5 \times 10^{-4}$ s), dissociating products should be able to rearrange to their low-energy conformations after collisional excitation.

Computational Details. All of the neutral ligands and metalated complexes investigated here may have numerous geometric conformations with relative energies close to the lowest-energy complex. To find the global minimum energy and all low-energy geometries, a large number of possible conformations were screened as follows.[18] A simulated annealing methodology using the AMBER suite of programs and the AMBER force field[41] was used to generate starting structures for higher-level optimizations. All unique structures generated via simulated annealing were further optimized using NWChem[42] at the HF/3-21G level. All unique structures from the HF/3-21G calculations within about 30 kJ/mol of the lowest-energy structure (up to ~10 structures for each $Na^+(L)$ complex) were further optimized using Gaussian 03[43] at the B3LYP/6-31G(d) level with "loose" optimization (maximum step size of 0.01 au and a rms force of 0.0017 au) to facilitate more rapid convergence. All unique structures were then optimized at the B3LYP/6-311+G(d,p) level. Rotational constants were obtained from the optimized structures, and vibrational frequencies were also calculated at this level. When used in internal energy determinations or for RRKM calculations, the vibrational frequencies were scaled by 0.99.[44] Single-point energies were calculated at the MP2(full), B3LYP, and B3P86 levels using the 6-311+G(2d,2p) basis set and the B3LYP/6-311+G(d,p) geometries. Zero-point vibrational energy (ZPE) corrections were determined using the scaled vibrational frequencies. Basis set superposition errors (BSSE) were estimated using the full counterpoise (cp) method.[45,46] Feller and co-workers[47,48] and Ohannesian and co-workers[49,50] have previously commented that the full counterpoise approximation to BSSE for MP2 calculations can provide worse agreement with experiment than MP2 values without BSSE corrections. Because of this possibility for BSSE to overcorrect the MP2 calculations, both values are reported here. Alternatively, observations by this lab[18,51] and others[52] find that BSSE corrections for DFT calculations on alkali metal cation systems are generally small. All of the absolute binding energies obtained using DFT calculations reported here include BSSE corrections.

Results

Cross Sections for Collision-Induced Dissociation. Experimental cross sections were obtained for the interaction of Xe with complexes formed by association of Na^+ with L = Asn, Gln, Asp, and Glu. To introduce these ligands into the gas phase, it was necessary to heat them to experimental temperatures in the range of the solid-phase melting temperatures of these amino acids, T_m = 185−270 °C. During these experiments, temperatures required in the flow tube to generate intense ion beams varied over 40 °C in the course of several hours, which led to variations in the relative magnitudes of the cross sections obtained. Therefore, the reaction channels for all data sets were normalized in intensity to a representative magnitude prior to data analysis in order to provide accurate thermochemical information.

Figure 1 shows representative data sets for all four $Na^+(L)$ systems. Data shown are a mean of results for xenon pressures of ~0.04, 0.08, and 0.16 mTorr as no pressure dependence for these systems was observed. In these experiments, an HX loss channel is the dominant product for each $Na^+(L)$ complex, where HX = NH_3 for the amides and H_2O for the acids. Formation of $Na^+(HX)$ is a major product, and the declines in the $Na^+(L-HX)$ channel cross sections make it evident that these channels compete with formation of $Na^+(HX)$. Formation of Na^+ is observed as a minor channel except for the Asp system. The appearance of these cross sections differs dramatically from those obtained for $Na^+(L)$ complexes where the amino acid remains intact.[14] We rationalize these drastic variations in results by hypothesizing that the amino acids undergo thermal decomposition according to reaction 3 in the flow tube source, aided by the complexation energy to the sodium cation

$$Na^+ + L + \text{heat} \rightarrow Na^+(L-HX)(HX) \qquad (3)$$

This generates a bis-ligand structure, $Na^+(L-HX)(HX)$, composed of a sodium cation, the (L−HX) decomposition product where the nomenclature indicates that HX has been lost from L, and HX such that the bis-ligand complexes have masses equivalent to those of the $Na^+(L)$ complexes. Such bis-ligand structures would decompose by reactions 4−6, which explains why reaction 5 is observed here (but not for intact $Na^+(L)$ complexes), why both reactions 4 and 5 have low thresholds (much lower than that for $Na^+(L)$), why these processes compete

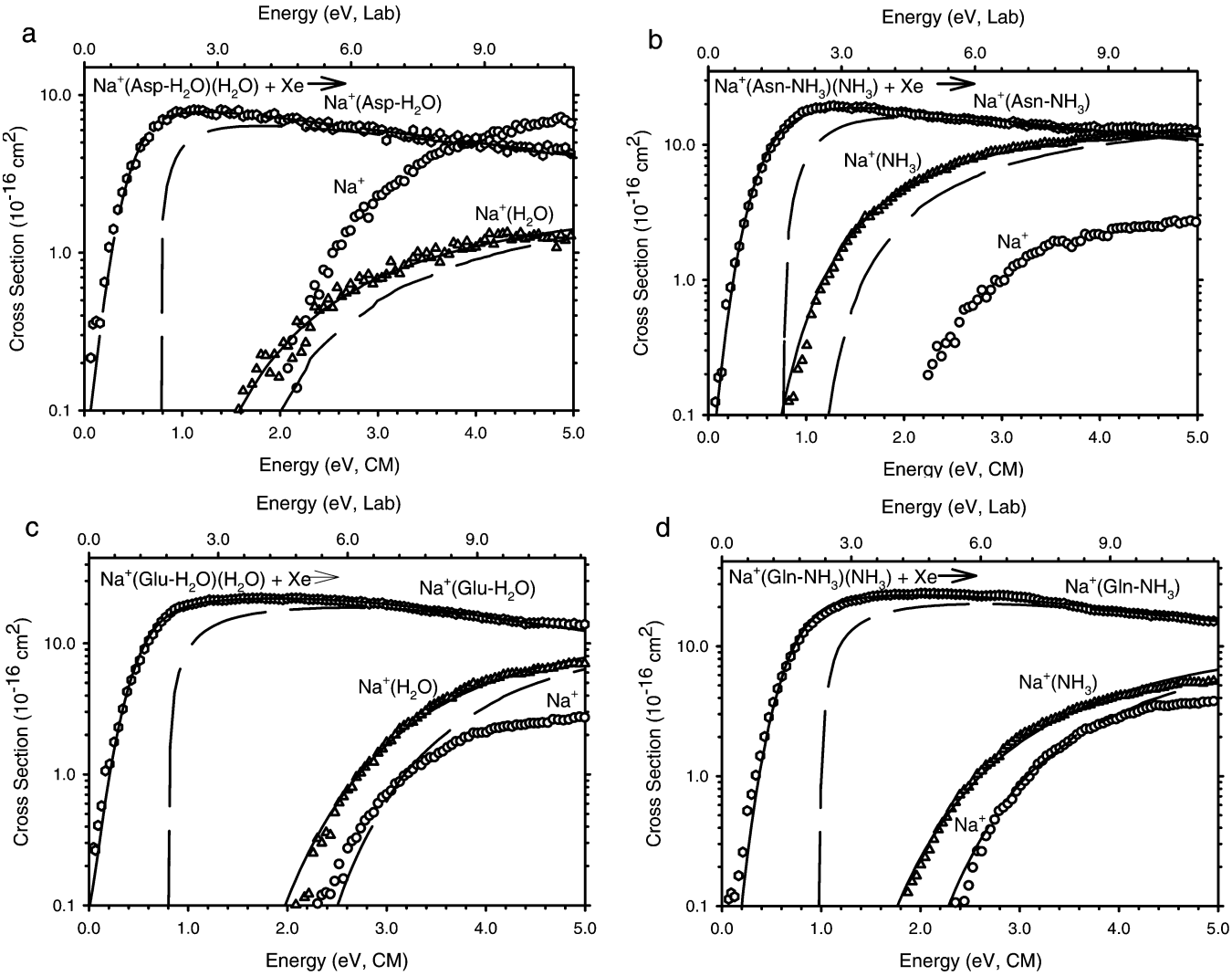

Figure 1. Cross sections for collision-induced dissociation of $Na^+(L)$ created in the flow tube source by association of Na^+ with Asp, Asn, Glu, and Gln (parts a−d, respectively) with Xe as a function of kinetic energy in the center-of-mass frame (lower *x*-axis) and the laboratory frame (upper *x*-axis). Solid lines show the best fit to the data using the competitive model of eq 1 convoluted over the neutral and ion kinetic and internal energy distributions. Dashed lines show the model cross sections in the absence of experimental kinetic energy broadening for reactions with an internal energy of 0 K.

with one another, and why Na^+ production is generally inefficient (much less than that for $Na^+(L)$ complexes)[14]

$$Na^+(L\text{-}HX)(HX) + Xe \rightarrow Na^+(L\text{-}HX) + HX + Xe \quad (4)$$

$$\rightarrow Na^+(HX) + (L\text{-}HX) + Xe \quad (5)$$

$$\rightarrow Na^+ + (L\text{-}HX) + HX + Xe \quad (6)$$

Evidence for such a decomposition process is the observation of $Na^+(L-HX)$ complexes emanating from the source, although the intensities of these species are substantially lower than those of the purported $Na^+(L-HX)(HX)$ species and too small for independent TCID studies. The low intensity of these species is consistent with the hypothesis that the decomposition reactions are largely driven by sodium cation association with the amino acid, rather than being a result of decomposition of the amino acid followed by assembly of the bis-ligand complexes. Of course, some of the ions produced in the DC/FT source may correspond to intact $Na^+(L)$ complexes, but the behavior observed in Figure 1 is dominated by the higher-energy $Na^+(L-HX)(HX)$ species. It is possible that the magnitude of the observed atomic sodium cation channel in the DC/FT experiments is an indicator of the amount of the $Na^+(L)$ complex remaining in the ion beam. CID experiments of the intact $Na^+(L)$ complexes[14] demonstrate that $Na^+(Asp)$ decomposes less readily than the other three complexes, which is consistent with the observation that the magnitude of the sodium cation channel in the DC/FT data is considerably larger for the Asp system compared to that for the others. Quantitative comparison of the magnitudes of the Na^+ channels in the ESI[14] and DC/FT experiments suggest that $Na^+(Asp)$ could comprise up to 40% of the ions formed in the DC/FT source, whereas the intact amino acid complexes comprise less than 12−16% of the DC/FT ions for Asn, Glu, and Gln.

We also considered whether the dominant species formed in the DC/FT source might be high-energy conformers of the intact $Na^+(L)$ complexes. This would explain why the threshold for reaction 4 moves to lower energy. However, a high-energy conformer should also allow formation of Na^+ shifted to lower energy by the same amount as the decomposition products, whereas the Na^+ thresholds observed here are either the same or only slightly lower than those from the ESI data. Furthermore, the decomposition reactions 4 and 5 from such conformers are

likely to occur by passing over a tight, rate-limiting transition state, which would result in all products having the same threshold energy, which is clearly not the behavior observed here, Figure 1. If these tight TSs were lower in energy than the asymptotic energies of the products (which would also mean that they are no longer rate-limiting), then the behavior observed for an excited conformer should parallel that observed in the ESI experiments,[14] but with less energy needed to induce the observed reactions, which is not the case. If one imagines that the purported excited conformations behaved differently than the isoenergetic ground-state conformers of $Na^+(L)$ formed by collisional excitation, that is, that these conformers explore different regions of phase space, then it becomes difficult to imagine why the excited-state conformers would be formed preferentially in the DC/FT source, which routinely forms metal cation complexes in their ground states. In contrast, the bis-ligand complexes, being distinct isomers of the $Na^+(L)$ complexes, do explore different regions of phase space because they need to pass back over a high-energy tight TS to re-form the intact amino acid complex. Importantly, once this rearrangement occurs in the DC/FT source, there are sufficient collisions with the flow gases to stabilize and thermalize the bis-ligand isomer, which the data analysis below demonstrates.

Decomposition Pathways for $Na^+(L)$. Complexes of ions formed in the DC/FT source are clearly no longer intact $Na^+(L)$ complexes but have undergone processes related to decomposition of the amino acids by loss of HX. Likely candidates for these decompositions can be identified by referring to the literature. Analogous decompositions of Asx residues have been observed to occur by loss of their terminal functionality on the side chain (H_2O and NH_3) under physiological conditions[9,10] and also for protonated Asx derivatives in the gas phase,[11] where it was proposed that a five-membered succinic ring structure is formed. Additionally, gas-phase cleavages at aspartic acid residues of sodiated peptides are observed to occur via a salt-bridge mechanism to form an analogous cyclization cleavage product.[53] Most interestingly, the loss of ammonia from asparaginyl residues under physiological conditions forms a five-membered ring succinimide via this type of cyclization, a process that has been linked to the process of biological aging.[1,2] In the isolated Asn system, the analogue of these cyclizations forms the 3-amino succinic anhydride (a-SA) molecule shown in Figure 2.

For the longer-chain amino acids, there have been several schemes elucidated for how Glx amino acids lose H_2O or NH_3 in different environments. It is known that formation of a five-membered ring lactam molecule, oxo-proline (O-Pro), Figure 2, occurs readily in aqueous solutions of glutamic acid[54] and glutamine[55] via HX loss. In the gas phase, protonated Glx amino acids undergoing CID lead to a mixture of products associated with HX loss, including oxo-proline, a protonated six membered ring imide from Glx, an analogous six-membered ring lactam from Gln, as well as ketene-like products for both Glx amino acids.[12] Each of these fragment structures (F2-Glx, F1-Glx, F4-Gln, and F3-Glx, respectively, where the nomenclature indicates a particular fragment originating from an amino acid) is shown in Figure 2, as well as their analogues for the shorter-chain Asx amino acids.

To identify the structure of the decomposition complexes observed in our experiments, as formed in reactions 3, the prospective (L−HX) molecules shown in Figure 2 were investigated computationally. Quantum chemical calculations for each decomposition reaction were completed as detailed in the computational section above, and the results are provided

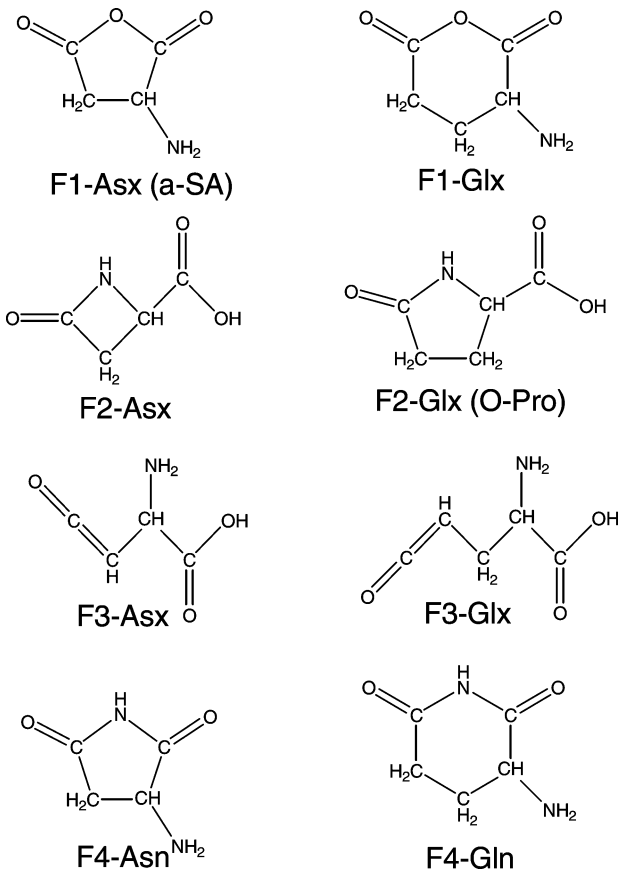

Figure 2. Possible structures for fragments resulting from HX loss from the Asx and Glx amino acids.

TABLE 1: Theoretical Energies (kJ/mol) for $Na^+(L)$ Decomposition[a]

reactions	B3LYP	B3P86	MP2(full)
Na^+(Asp) → Na^+(F1-Asx)(H_2O)	**39**	**45**	**43**
→ Na^+(F2-Asx)(H_2O)	50	55	63
→ Na^+(F3-Asx)(H_2O)	100	121	108
Na^+(Glu) → Na^+(F1-Glx)(H_2O)	49	54	50
→ Na^+(F2-Glx)(H_2O)	**−25**	**−25**	**−28**
→ Na^+(F3-Glx)(H_2O)	85	104	90
Na^+(Asn) → Na^+(F1-Asx)(NH_3)	**54**	**61**	**64**
→ Na^+(F2-Asx)(NH_3)	64	70	83
→ Na^+(F3-Asx)(NH_3)	115	137	129
→ Na^+(F4-Asn)(H_2O)	6	9	8
Na^+(Gln) → Na^+(F1-Glx)(NH_3)	64	70	70
→ Na^+(F2-Glx)(NH_3)	**−19**	**−17**	**−8**
→ Na^+(F3-Glx)(NH_3)	102	122	112
→ Na^+(F4-Gln)(H_2O)	0	1	−4

[a] Calculations performed at the stated level of theory using a 6-311+G(2d,2p) basis set with geometries calculated at the B3LYP/6-311+G(d,p) level. Energies for the $Na^+(L)$ reactants are taken from Heaton et al.[14] Reactions in bold are the likely decomposition pathways; see text. Italicized reactions correspond to water loss from the carboxamide amino acids, Asn and Gln.

in Table 1. The specified energies refer to the overall energetics for each reaction and neglect the possibility that the decompositions are limited instead by higher-energy tight TSs. For the Asx amino acids, formation of a-SA (F1-Asx) is the lowest-energy pathway for H_2O loss from Asp and NH_3 loss from Asn by 9−20 kJ/mol, but it is an endothermic reaction. As noted above, in the DC/FT ion source, these decomposition reactions can be driven by the thermal energy of the heated ligand and the considerable energy released upon complexation with the sodium cation (>200 kJ/mol).[14] H_2O loss from Asn by formation of F4-Asn appears lower in energy than a-SA formation by ∼50

TABLE 2: Fitting Parameters of Equation 1, Threshold Dissociation Energies at 0 K, and Entropies of Activation at 1000 K for CID of $Na^+(L-HX)(HX)$ with Xe[a]

reactant	ionic product	σ_0	n	E_0 (PSL) (eV)	$\Delta S^{\ddagger}_{1000}$ (J/K/mol)
$Na^+(Asp-H_2O)(H_2O)$[b]	Na^+(a-SA)	10.8 (4.7)	0.6 (0.1)	0.75 (0.06)	−7 (5)
	$Na^+(H_2O)$	11.2 (4.9)		1.12 (0.04)	31 (5)
$Na^+(Asn-NH_3)(NH_3)$[b]	Na^+(a-SA)	31.8 (5.4)	0.9 (0.1)	0.76 (0.04)	−4 (5)
	$Na^+(NH_3)$	154 (6.0)		1.03 (0.05)	25 (5)
$Na^+(Glu-H_2O)(H_2O)$[c]	Na^+(O-Pro)	33.1 (4.7)	0.7 (0.1)	0.79 (0.05)	20 (5)
	$Na^+(H_2O)$	29600 (770)		1.54 (0.06)	44 (5)
$Na^+(Gln-NH_3)(NH_3)$[c]	Na^+(O-Pro)	40.4 (4.9)	0.7 (0.1)	0.91 (0.04)	−8 (5)
	$Na^+(NH_3)$	3610 (55)		1.45 (0.04)	8 (5)

[a] Uncertainties in parentheses. [b] Analyzed using molecular parameters appropriate for a-SA (F1-Asx). [c] Analyzed using molecular parameters appropriate for O-Pro (F2-Glx).

kJ/mol by this analysis; however, this product is not observed experimentally in the collision-induced dissociation of Na^+(Asn),[14] such that its formation likely involves a high-energy TS. For both Glx amino acids, O-Pro (F2-Glx) formation is the lowest-energy pathway for HX loss by over 74 kJ/mol at all levels of theory and is the only exothermic pathway. H_2O loss from Gln by formation of F4-Gln is close in energy to O-Pro formation but still less favorable by 4−19 kJ/mol. Overall, the results of Table 1 and our experimental findings suggest that the (L−HX) decomposition products correspond to a-SA (F1-Asx) for Asp and Asn and O-Pro (F2-Glx) for Glu and Gln. The likelihood of these particular pathways is also bolstered because they parallel those proposed for analogous decompositions in the literature, as reviewed above.

Threshold Analysis of DC/FT Source Data. Equation 1 was used to analyze the competitive thresholds for reactions 4 and 5 for all four $Na^+(L-HX)(HX)$ systems. Figure 1 shows the experimental cross sections modeled assuming (L−HX) = a-SA for the Asx amino acids and (L−HX) = O-Pro for the Glx amino acids. The cross sections in Figure 1 are reproduced by eq 1 over a large range of energies (>4 eV) and magnitudes (about 2 orders of magnitude). The results of these analyses are provided in Table 2. Comparable reproduction of the data is obtained using molecular parameters of the alternate (L−HX) fragments: F2-Asx, F3-Asx, F1-Glx, and F3-Glx. These fitting results are provided in Table S1 of the Supporting Information. The threshold energies are not particularly sensitive to the fragment assumed in the analysis, with thresholds usually differing by less than 0.05 eV and in no case by more than 0.15 eV. Thus, similar thermochemistry is obtained for all possible fragments, as discussed in more detail below.

For data modeling, independent $\sigma_{0,j}$ values for each channel are used in order to reproduce the experimental data when using the competitive analysis, as previously utilized for a number of studies of competitive dissociations.[35,56,57] The use of independent scaling factors compensates for neglected factors, such as reaction degeneracies, symmetry numbers of the reactant and product molecules, dipole moments of neutral products, and inaccurate estimations of metal−ligand frequencies, although all of these factors are included in the modeling to the best of our ability to estimate them. In the present study, independent scaling factors were used to fit the $Na^+(L-HX)(HX)$ systems because the data could not be accurately reproduced without them. Table 2 shows that the scaling factors ascertained for the minor Na^+(HX) product channel were found to exceed those for the major $Na^+(L-HX)$ channel by 1−5 for the Asx complexes and 100−1000 for the Glx complexes. The former relative values are consistent with previous work, whereas the magnitudes of the latter values are notably larger than those required in previous studies.[35,56,57] The tighter binding and larger number of molecular degrees of freedom in the complexes derived from Glx is probably related to the explanation for the larger relative scaling factors for these systems compared to those for the smaller Asx systems and those studied previously. Ultimately, whatever their origins, it is not possible to accurately reproduce the experimental results without independent scaling factors. Furthermore, as discussed in the following, the thermochemistry obtained is quite reasonable, leading us to conclude that our threshold interpretations are reasonable.

The relative thresholds for reactions 4 and 5 can be combined to determine the sodium cation binding affinities for the (L−HX) fragments. This simply recognizes that the sum of the bond energies for removing both ligands from the $Na^+(L-HX)$-(HX) complexes does not depend on the order in which the ligands are removed, that is

$$D[(L-HX)Na^+-HX] + D[Na^+-(L-HX)] = D[(HX)Na^+-(L-HX)] + D(Na^+-HX) \quad (7)$$

which can be rearranged to

$$D[Na^+-(L-HX)] = D[(HX)Na^+-(L-HX)] - D[(L-HX)Na^+-HX] + D(Na^+-HX) \quad (8)$$

Here, $D[(L-HX)Na^+-HX]$ and $D[(HX)Na^+-(L\text{-}HX)]$ are taken as equivalent to the thresholds for reactions 4 and 5, respectively, and the absolute Na^+-L bond dissociation enthalpies for $Na^+(H_2O)$ and $Na^+(NH_3)$, 91.2 ± 6.3 and 106.2 ± 5.7 kJ/mol, are taken from Amicangelo and Armentrout.[58] It is also useful to note that the relative thresholds for reactions 4 and 5, that is, $D[(HX)Na^+-(L-HX)] - D[(L-HX)Na^+-HX]$, are more precisely determined than either absolute threshold because a number of uncertainties cancel. The uncertainties in these relative thresholds are 3−6 kJ/mol in the Asx cases and 5−7 kJ/mol in the Glx cases. The sodium cation affinities of (Asx−HX) obtained from the $Na^+(Asp-H_2O)(H_2O)$ and $Na^+(Asn-NH_3)(NH_3)$ systems assuming the fragment is a-SA (F1-Asx) are in good agreement with one another, 127 ± 9 and 133 ± 7 kJ/mol, respectively, Table 3. For (Glx−HX), the sodium cation affinities obtained from the $Na^+(Glu-H_2O)(H_2O)$ and $Na^+(Gln-NH_3)(NH_3)$ systems assuming an O-Pro (F3-Glx) fragment also agree well, 167 ± 9 and 158 ± 8 kJ/mol, respectively, Table 3. The BDEs derived for a-SA and O-Pro are a weighted average of both values obtained for each ligand, 130 ± 5 and 161 ± 6 kJ/mol, respectively, where the uncertainties are two standard deviations of the mean. Comparable information for analysis of all systems assuming each possible fragment is collected in Table S2. In the Asx systems, if the data are analyzed assuming that the fragments are F2-Asx or F3-Asx, the weighted average BDEs obtained are nearly the same as that for a-SA, 131 ± 8 and 129 ± 6 kJ/mol, respectively. For the Glx systems, analyses assuming the F1-

TABLE 3: Experimental and Theoretical Reaction Energies (kJ/mol) for Decomposition of $Na^+(L-HX)(HX)$ Complexes Formed in the DC/FT Source and for $Na^+(L-HX)$ Complexes

reactant	product	TCID[a]	B3LYP[b]	B3P86[b]	MP2 (full)[b]
$Na^+(Asp-H_2O)(H_2O)$	Na^+(a-SA)	72 (6)	77	74	78
	$Na^+(H_2O)$	108 (4)	119	115	119
Na^+(a-SA)	Na^+	127 (9)	138	133	134
$Na^+(Asn-NH_3)(NH_3)$	Na^+(a-SA)	73 (4)	87	85	88
	$Na^+(NH_3)$	99 (5)	114	110	115
Na^+(a-SA)	Na^+	133 (7)	138	133	134
$Na^+(Glu-H_2O)(H_2O)$	Na^+(O-Pro)	76 (5)	68	67	78
	$Na^+(H_2O)$	149 (6)	139	136	145
Na^+(O-Pro)	Na^+	167 (9)	167	162	160
$Na^+(Gln-NH_3)(NH_3)$	Na^+(O-Pro)	88 (4)	88	86	88
	$Na^+(NH_3)$	140 (4)	144	140	141
Na^+(O-Pro)	Na^+	158 (8)	167	162	160

[a] Threshold values taken from Table 2 and $Na^+(L-HX)$ bond energies derived using eq 8. Uncertainties in parentheses. [b] Single-point energies calculated at the level of theory shown using a 6-311+G(2d,2p) basis set and structures and ZPEs determined at the B3LYP/6-311+G(d,p) level of theory. Counterpoise corrections are not included.

Glx and F3-Glx fragments yield weighted average BDEs of 168 ± 8 and 163 ± 8 kJ/mol, slightly higher than the O-Pro value. These values can now be used for a final identification of the fragments by comparison with theoretical values for the various fragments, as detailed below.

Theoretical Results for $Na^+(L-HX)$ and $Na^+(L-HX)(HX)$ Complexes. Theoretical bond energies for loss of HX and (L−HX) from the $Na^+(L-HX)(HX)$ complexes and those for $Na^+(L-HX)$ are compared to the experimental thresholds and $D_0[Na^+(L-HX)]$ values derived using eq 8 in Tables 3 and S2. As noted above, the experimental threshold energies are not overly sensitive to which particular fragment is used in the analysis, such that these comparisons can be used to assess which fragment is formed. Among the various possibilities, the best agreement between experiment and theory is found for F1-Asx (a-SA) in both the Asp and Asn systems and for F2-Glx (O-Pro) in both the Glu and Gln systems. Summarizing these comparisons, when the a-SA fragment is used in analyzing the Asx systems, the difference between the six resulting experimental values and theory at three different levels, Table 3, has a mean absolute deviation (MAD) of 8 kJ/mol, whereas the alternate fragments, F2-Asx and F3-Asx, yield MADs of 36 and 22 kJ/mol, respectively, Table S2. Likewise, when molecular parameters for O-Pro are used to analyze the Glx systems, the MAD is 4 kJ/mol, compared to 21 and 11 kJ/mol for F1-Glx and F3-Glx, respectively. Significantly, the good agreement between experiment and theory (within experimental error) for the a-SA and O-Pro analyses also supports the identification of the species formed in the DC/FT source as having the $Na^+(L-HX)(HX)$ structures.

Figure 3 shows this comparison more pictorially by plotting the experimental and theoretical sodium cation affinities for each possible (L−HX) species, where perfect agreement is indicated by the diagonal line. It is clear that F2-Asx and F3-Asx have much greater calculated Na^+ binding affinities than the reactant observed in the flow tube, whereas the binding affinity calculated for F1-Asx (a-SA) correlates with experiment very well. Further, the assignment of a-SA as the fragment is consistent with the low-energy decomposition processes outlined in Table 1. For the Glx systems, F3-Glx is calculated to bind sodium cations more tightly and F1-Glx more weakly than the experimentally observed fragment, whereas F2-Glx (O-Pro) binding correlates very well. Again, this agrees with the

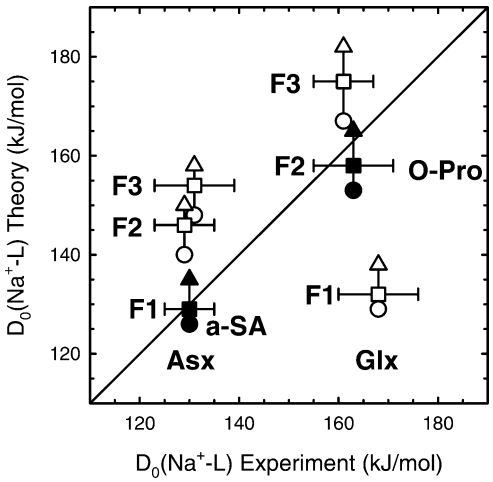

Figure 3. Experimental versus theoretical bond energies (kJ/mol) of sodium cations for the fragments resulting from HX loss from the Asx and Glx amino acids. Theoretical values include those calculated at the B3LYP (triangles), B3P86 (squares), and MP2(full,cp) (circles) levels of theory. Good agreement between experiment and theory is indicated by the solid points for a-SA (F1-Asx) and O-Pro (F2-Glx). All values are from Table S2.

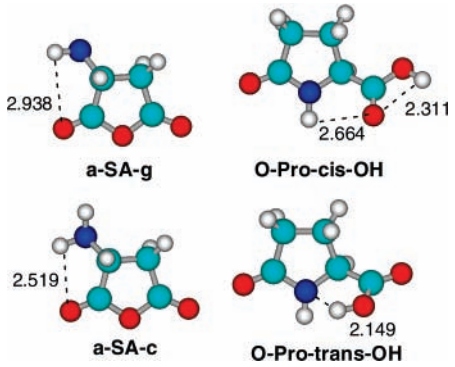

Figure 4. Low-energy structures of neutral a-SA and neutral O-Pro calculated at the B3LYP/6-311+G(d,p) level of theory. Hydrogen bond lengths are shown in Å.

TABLE 4: Ground- and Excited-State Energies (kJ/mol) for Neutral a-SA and O-Pro[a]

species	B3LYP	B3P86	MP2(full)
a-SA-g	0.0	0.0	0.0
a-SA-c	0.6	0.2	0.1
O-Pro−*cis*-OH	0.0	0.0	0.0
O-Pro−*trans*-OH	13.3	11.9	11.1

[a] Calculations performed at the stated level of theory using a 6-311+G(2d,2p) basis set with geometries and zero-point energies calculated at the B3LYP/6-311+G(d,p) level.

energetics for decomposition shown in Table 1. Overall, these results establish that the DC/FT source produces the Na^+(a-SA)(HX) and Na^+(O-Pro)(HX) complexes.

Our molecular dynamic simulations generate only two low-energy structures for both a-SA and O-Pro, as shown in Figure 4 and Table 4. This is not surprising as the ring structure of each molecule greatly restricts its conformational flexibility. For a-SA, the two structures contain their ring in a low-energy puckered conformation and differ only by rotation of the substituent amino group (labeled g for gauche and c for cis according to the ∠HNCC dihedral angle), providing an energy difference of <1 kJ/mol, Table 4. Both low-energy structures are able to form a hydrogen bond between the amino hydrogen and a carbonyl oxygen of the ring. The two low-energy structures of O-Pro are similar in their ring conformation but

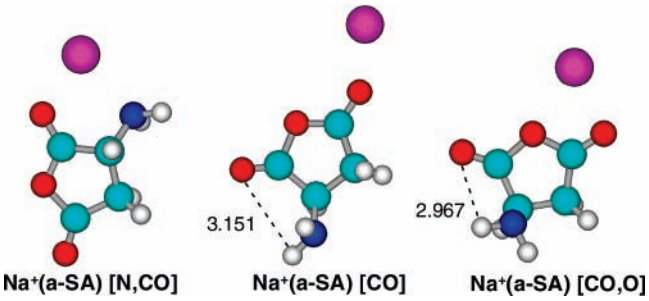

Figure 5. Low-energy structures of sodiated a-SA calculated at the B3LYP/6-311+G(d,p) level of theory. Hydrogen bond lengths are shown in Å.

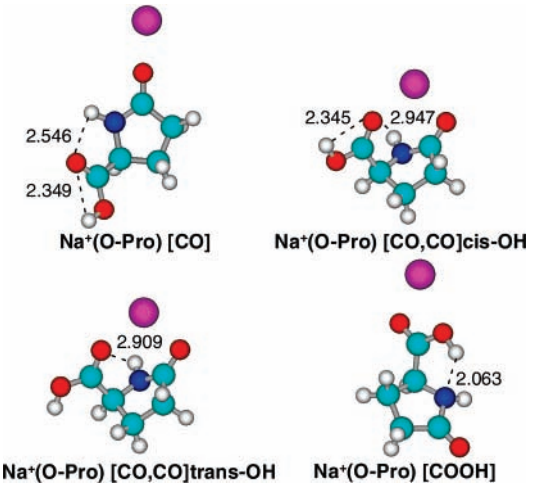

Figure 6. Low-energy structures for sodiated O-Pro calculated at the B3LYP/6-311+G(d,p) level of theory. Hydrogen bond lengths are shown in Å.

differ by rotation of their substituent carboxylic acid group, providing a more significant energy difference of 11−13 kJ/mol. In the *cis*-OH ground state, the carboxylic acid group extends away from the ring and hydrogen bonds to itself, Figure 4. In the higher-energy *trans*-OH structure, the carboxylic acid group orients in a less sterically favored conformation, loses its internal hydrogen bond, but is stabilized by forming a hydrogen bond to the nitrogen of the ring.

Introducing a Na^+ metal complicates things considerably such that a number of low-energy structures are generated for each system. The [N,CO] GS of Na^+(a-SA), where the brackets indicate the Na^+ binding sites, binds sodium in a bidentate association with the substituent amino group and nearest carbonyl oxygen, Figure 5. The [CO] and [CO,O] structures each bind the sodium cation through associations with the oxygen atoms of the molecule, which fail to stabilize the sodium cation's positive charge as effectively, as indicated by higher energies of 12−16 kJ/mol, Table 5. The [CO] GS of Na^+(O-Pro) binds the sodium cation in a monodentate configuration along the dipole of its ring carbonyl oxygen, Figure 6, with the conformation of O-Pro being nearly identical to the GS of the neutral molecule. Binding of metal cations along the dipoles of carbonyl groups strongly stabilizes these interactions for monodentate coordination,[18] and maintenance of the ground-state O-Pro configuration clearly stabilizes the complex. The Na^+(O-Pro) structure next highest in energy, [CO,CO]*cis*-OH, solvates the sodium cation in a bidentate association with both carbonyl oxygens. Although stabilization of the sodium cation interaction is clearly enhanced by the coordinated solvation of two heteroatoms, the conformational strain required to achieve these interactions by O-Pro is extreme enough that this structure is essentially isoenergetic with the monodentate [CO] conformation, lying 2.4 kJ/mol lower to 4.5 kJ/mol higher in energy. A similar structure, [CO,CO]*trans*-OH, differs from [CO,CO]*cis*-OH only in the orientation of the terminal −OH in the carboxylic group of the amino acid backbone. Where the cis conformer allows for H-bonding with the carbonyl oxygen, this interaction is not possible in the trans conformer, resulting in it being ∼18−23 kJ/mol higher in energy. We also located a bidentate association of the sodium cation bridged between the oxygen atoms of the substituent carboxylic acid functionality, [COOH], but this lies 43−47 kJ/mol above the GS conformation.

For the GS of the bis-ligand complexes, Na^+(a-SA)(HX) and Na^+(O-Pro)(HX), the calculated GS structures are analogous to the GS of Na^+(a-SA) and Na^+(O-Pro), with the addition of a H_2O or NH_3 molecule on the opposite side of the sodium cation.

The alternative fragments considered above have GSs that involve similar binding schemes, as shown in Figure S1 and Table S3 in the Supporting Information. F2-Asx binds the sodium cation most favorably along the dipole of the carbonyl substituent of its ring like its O-Pro [CO] analogue, whereas F1-Glx binds the sodium cation most favorably in a bidentate association with the amino group nitrogen and adjacent carbonyl oxygen of the ring like its a-SA [N,CO] analogue. The F3-Asx/Glx fragments each bind the sodium cation in a tridentate association with the amino nitrogen and both carbonyl oxygens. In these cases, the [N,CO,CO] binding schemes most closely resemble those for the ground states of the sodiated intact amino acids.[14] Last, the F4-Asn/Gln fragments both bind the sodium cation bidentate with the amino group nitrogen and adjacent carbonyl oxygen of the ring, analogous to the a-SA and F1-Glx [N,CO] binding orientations.

In assessing the trends in the calculated sodium cation binding affinities of these various fragments, Figure 3, it is clear that the F3 fragments have the highest bond energies because of their tridentate configuration, with the longer-chain F3-Glx having a higher bond energy because it is less sterically constrained than the shorter-chain F3-Asx. Interestingly, the calculated bond energies for F1-Asx (a-SA) and F1-Glx are similar, consistent with a very similar [N,CO] binding configuration. In contrast, F2-Asx has a weaker binding affinity than F2-Glx (O-Pro), which can be traced to the severe steric restrictions associated with the four-membered ring of F2-Asx. This prevents the bidentate [CO,CO] configuration that is low-lying for O-Pro, Figure 6, and reduces the strength of the NH···OC hydrogen bond that stabilizes the [CO] conformation of Na^+(O-Pro) (2.55 vs 2.97 Å in Na^+(F2-Asx)).

Discussion

Conversion from 0 to 298 K and Excited Conformers. Conversion from 0 K bond energies to 298 K bond enthalpies and free energies is accomplished using the rigid rotor/harmonic oscillator approximation with rotational constants and vibrational frequencies calculated at the B3LYP/6-311+G(d,p) level. These ΔH_{298} and ΔG_{298} values along with the conversion factors and 0 K enthalpies measured here are reported in Table 6. The uncertainties listed are determined by scaling most of the vibrational frequencies by ±10% along with twofold variations in the metal−ligand frequencies. We also calculated the ΔG_{298} values for the second lowest-energy structure of all systems considered here. In general, the relative ΔG_{298} excitation energies are comparable to the analogous differences in the ΔH_0 values, Table 5.

The theoretical BDEs discussed below are all calculated for the most stable geometric conformation of each reactant species.

TABLE 5: Bond Distances (Å), Bond Angles (°), and Relative Energies (kJ/mol) for Low-Energy Structures of Sodiated a-SA and O-Pro[a]

species	$r(Na^+-O)^b$	$r(Na^+-N)$	$r(Na^+-O)$	$\angle(O^bNaX)$	B3LYP	B3P86	MP2(full)
Na^+(a-SA) [N,CO]	2.247	2.532		73.1[c]	0.0	0.0	0.0
[CO]	2.161				12.5	13.0	16.4
[CO,O]	2.312		2.517[d]	54.4[d]	13.0	13.1	15.7
Na^+(O-Pro) [CO]	2.097				0.0	0.0	2.4
[CO,CO]*cis*-OH[e]	2.281	3.308	2.349[f]	94.0[f]	4.5	3.1	0.0
[CO,CO]*trans*-OH[e]	2.298	3.372	2.311[f]	91.6[f]	23.1	21.2	18.0
[COOH]	2.264		2.607[g]	53.1[g]	47.0	44.6	43.4

[a] Calculations performed at the stated level of theory using a 6-311+G(2d,2p) basis set with geometries and zero-point energies calculated at the B3LYP/6-311+G(d,p) level. [b] Carbonyl oxygen. [c] Amino nitrogen. [d] Ring oxygen. [e] Terminal hydrogen of carboxylic acid. [f] Carbonyl oxygen of the carboxylic acid. [g] Hydroxyl oxygen of the carboxylic acid.

TABLE 6: Enthalpies and Free Energies of Binding at 0 and 298 K (kJ/mol)[a]

complex	$\Delta H_0{}^b$	$\Delta H_{298} - \Delta H_0{}^c$	ΔH_{298}	$T\Delta S_{298}{}^c$	ΔG_{298}
Na^+-(a-SA)	130 (5)	2.3 (0.3)	132 (5)	34.1 (4.8)	98 (7)
Na^+-(O-Pro)	161 (6)	1.3 (0.2)	162 (6)	30.0 (3.5)	132 (7)
Na^+(a-SA)$-(H_2O)$	72 (6)	0.1 (0.1)	72 (6)	27.8 (3.3)	44 (7)
Na^+(O-Pro)$-(H_2O)$	76 (5)	2.2 (0.3)	78 (5)	32.7 (4.6)	45 (7)
Na^+(a-SA)$-(NH_3)$	73 (4)	0.03 (0.01)	73 (4)	26.3 (4.6)	47 (6)
Na^+(O-Pro)$-(NH_3)$	88 (4)	0.17 (0.03)	88 (4)	26.2 (4.6)	62 (6)

[a] Uncertainties in parentheses. [b] Average experimental values from Table 3. [c] Calculated using standard formulas and molecular constants calculated at the B3LYP/6-311+G(d,p) level.

TABLE 7: Experimental and Theoretical Bond Energies at 0 K (kJ/mol)

complex	experiment[a]	B3LYP[b,c]	B3P86[b,c]	MP2(full)[b]	MP2(full,cp)[b,c]
Na^+-(a-SA)	130 (5)	135	129	134	126
Na^+-(O-Pro)	161 (6)	165	158	160	153
Na^+(a-SA)$-(H_2O)$	72 (6)	73	71	78	71
Na^+(O-Pro)$-(H_2O)$	76 (5)	65	64	78	71
Na^+(a-SA)$-(NH_3)$	73 (4)	84	83	88	81
Na^+(O-Pro)$-(NH_3)$	88 (4)	86	84	88	82
MAD[d]		6 (4)	5 (5)	5 (6)	5 (3)

[a] Present experimental values from Table 3. Uncertainties in parentheses. [b] Calculations performed at the stated level of theory using a 6-311+G(2d,2p) basis set with geometries calculated at the B3LYP/6-311+G(d,p) level. [c] Counterpoise corrected. [d] Mean absolute deviation from present experimental values.

For some of the systems, it is possible that the complexes formed experimentally in the source region at thermal energies may consist of multiple low-energy conformers. Although no obvious evidence for multiple conformers is found experimentally, the sensitivity of TCID experiments to low-energy species is not particularly acute. Using the ΔG_{298} values to calculate an equilibrium population of conformers shows that the calculated GS structures for most Na^+(L−HX)(HX) systems should be dominant in the room-temperature ion sources. Excited conformers are calculated to comprise 13−37% of the total Na^+(a-SA)(H_2O) population, 2−8% of the total Na^+(a-SA)(NH_3) population, 1−22% of the total Na^+(O-Pro)(H_2O) population, and 0.1−2% of the total Na^+(O-Pro)(NH_3) population (depending on the level of theory). To investigate the effect of having a different conformer populating the Na^+(L−HX)(HX) reactant ions, we reanalyzed the data using the molecular parameters of the second lowest-energy structure for these systems. The threshold energies change by less than 1 kJ/mol in all cases, an effect that is included in the uncertainties listed in the tables. Thus, even if there are multiple conformers present in the reactant ion beams, this does not affect the thermochemistry derived within the stated experimental uncertainties.

Comparison of Experimental and Theoretical Values. The sodium cation affinities for a-SA and O-Pro and the H_2O and NH_3 affinities of Na^+(a-SA) and Na^+(O-Pro) as measured using TCID with the guided ion beam mass spectrometer and calculated here are provided in Table 7. In all cases, the calculated binding energies refer to the ground-state conformations of each system. The agreement between theory and experiment is extremely good. Theoretical calculations span the range of our experimentally determined values in all cases except for the Na^+(a-SA)$-(NH_3)$ system, where theory is $8-15 \pm 4$ kJ/mol higher, just outside of our experimental uncertainty. All levels of theory provide comparable descriptions of our experimentally determined values, with mean absolute deviations (MAD) from experiment of 5−6 kJ/mol. All of these variations are comparable to the average experimental uncertainty of ∼5 kJ/mol.

Qualitative Trends. The observed (L−HX) molecules are both five-membered heterocyclic ring structures distinguished primarily by the placement of their −COO− group. The a-SA contains this group within its ring structure, whereas O-Pro has its carboxylic acid functionality as a substituent on its ring. The strength of sodium cation binding to the five-membered ring decomposition products is weaker than sodium cation binding to the intact amino acid complexes from which they are derived, where each involves a tridentate binding association with the sodium cation.[14] This is primarily a consequence of the conformational constraints that the ring structures play in their ability to bind the sodium cation, which results in bidentate and monodentate (or bidentate) binding to a-SA and O-Pro, respectively. Between the two cyclic structures, the monodentate Na^+(O-Pro) complex binds sodium more strongly than the bidentate Na^+(a-SA) complex. The strong stabilization that occurs in monodentate binding along the dipole of a carbonyl oxygen has been observed previously for similar systems,[18] where the benefit of bidentate binding must be sufficient to overcome the decrease in stability that occurs as the metal ion

bends away from binding along the dipole of the carbonyl. The lowest-energy bidentate structure of Na^+(O-Pro), [CO,CO]*cis*-OH, is also very stable and lies within 5 kJ/mol of the GS structure, Table 5. In a-SA, the amino group is naturally positioned on the ring to afford effective bidentate association with the sodium cation. Additionally, it has been noted that species such as NH_3, CH_3NH_2, and $C_3H_7NH_2$ bind to Na^+ more strongly than the analogous H_2O, CH_3OH, and C_3H_7OH ligands.[18,58,59] This trend is also observed here for H_2O and NH_3 binding to Na^+(a-SA) and Na^+(O-Pro), where NH_3 binds to these complexes more strongly than H_2O does, Table 7.

Conclusion

The kinetic energy dependence of the collision-induced dissociation of decomposed Na^+(L), where L = aspartic acid, glutamic acid, asparagine, and glutamine, with Xe is examined in a guided ion beam mass spectrometer. Complexes of the intact amino acids with the sodium cation readily decompose during formation in the flow tube ion source to form bis-ligand complexes, Na^+(L−HX)(HX), where HX = NH_3 for Asn and Gln and H_2O for Asp and Glu. Thresholds at 0 K for the Na^+ affinity of the (Asx−HX) and (Glx−HX) decomposition products, as well as the H_2O and NH_3 affinities of the Na^+(Asx−HX) and Na^+(Glx−HX) complexes, are determined after consideration of the effects of reactant internal energy, multiple collisions with Xe, and lifetime effects using a phase space limit transition-state model.[34] The experimental binding energies are in excellent agreement with quantum chemical calculations using the B3P86/6-311+G(2d,2p)//B3LYP/6-311+G(d,p) level of theory when (Asx−HX) is identified as a-SA and (Glx−HX) is identified as O-Pro but not for other possible fragments. This combined use of TCID experiments and theory demonstrates that complexes formed in the DC/FT source are primarily Na^+(a-SA)(HX) and Na^+(O-Pro)(HX) complexes. The bond dissociation energies (BDEs) reported here constitute the first direct experimental measurements of the sodium cation binding affinities to a-SA and O-Pro and the H_2O and NH_3 affinities of the Na^+(a-SA) and Na^+(O-Pro) complexes. By comparison with theory, the binding energies establish the ground-state conformations of these complexes. As these decomposition products provide less conformational mobility for sodium cation solvation than do the amino acids from which they are derived, they exhibit monodentate and bidentate associations with the sodium cations and substantially smaller binding affinities in comparison to the more strongly bound tridentate associations of the intact Asx and Glx amino acids.[14] Significantly, the identification of the deamidation and hydrolysis products of the Asx and Glx amino acids as the five-membered cyclic species, a-SA and O-Pro, respectively, is consistent with previous studies in both the solution and the gas phases.[9−12,53−55] The present work therefore provides some of the first quantitative information about these species and their interactions with biologically relevant Na^+, H_2O, and NH_3.

Acknowledgment. This work is supported by the National Science Foundation. A grant of computer time from the Center for High Performance Computing at the University of Utah is gratefully acknowledged.

Supporting Information Available: Tables of data analysis and structural parameters for all possible (Asx−HX) and (Glx−HX) fragments. A figure showing ground-state conformations of Na^+ complexes with alternate fragments. This material is available free of charge via the Internet at http://pubs.acs.org.

References and Notes

(1) Clarke, S. *Ageing Res. Rev.* **2003**, *2*, 263.
(2) Robinson, N. E.; Robinson, A. B. *Proc. Natl. Acad. Sci. U.S.A.* **2001**, *98*, 944.
(3) Shimizu, T.; Watanabe, A.; Ogawara, M.; Mori, H.; Shirasawa, T. *Arch. Biochem. Biophys.* **2000**, *381*, 225.
(4) Shimizu, T.; Fukuda, H.; Murayama, S.; Izumiyama, N.; Shirasawa, T. *J. Neurosci. Res.* **2002**, *70*, 451.
(5) Robinson, N. E.; Robinson, A. B. *J. Pept. Res.* **2004**, *63*, 437.
(6) Aswad, D. W. *Deamidation and Isoaspartate Formation in Peptides and Proteins*; CRC Press, Inc: Boca Raton, FL, 1995.
(7) Deverman, B. E.; Cook, B. L.; Manson, S. R.; Niederhoff, R. A.; Langer, E. M.; Rosova, I.; Kulans, L. A.; Fu, X.; Weinberg, J. S.; Heinecke, J. W.; Roth, K. A.; Weintraub, S. J. *Cell* **2002**, *111*, 51.
(8) Weintraub, S. J.; Manson, S. R. *Mech. Ageing Dev.* **2004**, *125*, 255.
(9) Capasso, S.; Mazzarella, L.; Sica, F.; Zagari, A.; Salvadori, S. *J. Chem. Soc., Perkin Trans.* **1993**, *2*, 679.
(10) Capasso, S.; Kirby, A. J.; Salvadori, S.; Sica, F.; Zagari, A. *J. Chem. Soc., Perkin Trans.* **1995**, *2*, 437.
(11) Harrison, A. G.; Tu, Y. *J. Mass Spectrom.* **1998**, *33*, 532.
(12) Harrison, A. G. *Int. J. Mass Spectrom.* **2001**, *210/211*, 361.
(13) Dayhoff, M. O. *Atlas of Protein Sequences and Structures*; National Biomedical Research Foundation: Silver Springs, MD, 1969.
(14) Heaton, A. L.; Moision, R. M.; Armentrout, P. B. *J. Phys Chem. A* **2008**, *112*, 3319.
(15) Ervin, K. M.; Armentrout, P. B. *J. Chem. Phys.* **1985**, *83*, 166.
(16) Muntean, F.; Armentrout, P. B. *J. Chem. Phys.* **2001**, *115*, 1213.
(17) Schultz, R. H.; Crellin, K. C.; Armentrout, P. B. *J. Am. Chem. Soc.* **1991**, *113*, 8590.
(18) Moision, R. M.; Armentrout, P. B. *J. Phys. Chem. A* **2002**, *106*, 10350.
(19) Moision, R. M.; Armentrout, P. B. *J. Am. Soc. Mass Spectrom.* **2007**, *18*, 1124.
(20) Dalleska, N. F.; Honma, K.; Armentrout, P. B. *J. Am. Chem. Soc.* **1993**, *115*, 12125.
(21) Dalleska, N. F.; Tjelta, B. L.; Armentrout, P. B. *J. Phys. Chem.* **1994**, *98*, 4191.
(22) Fisher, E. R.; Kickel, B. L.; Armentrout, P. B. *J. Phys. Chem.* **1993**, *97*, 10204.
(23) Khan, F. A.; Clemmer, D. E.; Schultz, R. H.; Armentrout, P. B. *J. Phys. Chem.* **1993**, *97*, 7978.
(24) Rodgers, M. T.; Armentrout, P. B. *J. Phys. Chem. A* **1997**, *101*, 1238.
(25) Teloy, E.; Gerlich, D. *Chem. Phys.* **1974**, *4*, 417.
(26) Gerlich, D. *Adv. Chem. Phys.* **1992**, *82*, 1.
(27) Aristov, N.; Armentrout, P. B. *J. Phys. Chem.* **1986**, *90*, 5135.
(28) Dalleska, N. F.; Honma, K.; Sunderlin, L. S.; Armentrout, P. B. *J. Am. Chem. Soc.* **1994**, *116*, 3519.
(29) Beyer, T. S.; Swinehart, D. F. *Commun. ACM* **1973**, *16*, 379.
(30) Stein, S. E.; Rabinovitch, B. S. *J. Chem. Phys.* **1973**, *58*, 2438.
(31) Stein, S. E.; Rabinovitch, B. S. *Chem. Phys. Lett.* **1977**, *49*, 183.
(32) Gilbert, R. G.; Smith, S. C. *Theory of Unimolecular and Recombination Reactions*; Blackwell Scientific: London, 1990.
(33) Robinson, P. J.; Holbrook, K. A. *Unimolecular Reactions*; Wiley-Interscience: New York, 1972.
(34) Rodgers, M. T.; Ervin, K. M.; Armentrout, P. B. *J. Chem. Phys.* **1997**, *106*, 4499.
(35) Rodgers, M. T.; Armentrout, P. B. *J. Chem. Phys.* **1998**, *109*, 1787.
(36) Hales, D. A.; Lian, L.; Armentrout, P. B. *Int. J. Mass Spectrom. Ion Processes* **1990**, *102*, 269.
(37) More, M. B.; Ray, D.; Armentrout, P. B. *J. Phys. Chem. A* **1997**, *101*, 7007.
(38) More, M. B.; Ray, D.; Armentrout, P. B. *J. Am. Chem. Soc.* **1999**, *121*, 417.
(39) Ye, S. J.; Armentrout, P. B. *J. Phys. Chem. B* **2008**, in press.
(40) Armentrout, P. B.; Simons, J. *J. Am. Chem. Soc.* **1992**, *114*, 8627.
(41) Pearlman, D. A.; Case, D. A.; Caldwell, J. W.; Ross, W. R.; Cheatham, T. E.; DeBolt, S.; Ferguson, D.; Seibel, G.; Kollman, P. *Comput. Phys. Commun.* **1995**, *91*, 1.
(42) Bylaska, E. J.; de Jong, W. A.; Kowalski, K.; Straatsma, T. P.; Valiev, M.; Wang, D.; Aprà, E.; Windus, T. L.; Hirata, S.; Hackler, M. T.; Zhao, Y.; Fan, P.-D.; Harrison, R. J.; Dupuis, M.; Smith, D. M. A.; Nieplocha, J.; Tipparaju, V.; Krishnan, M.; Auer, A. A.; Nooijen, M.; Brown, E.; Cisneros, G.; Fann, G. I.; Früchtl, H.; Garza, J.; Hirao, K.; Kendall, R.; Nichols, J. A.; Tsemekhman, K.; Wolinski, K.; Anchell, J.; Bernholdt, D.; Borowski, P.; Clark, T.; Clerc, D.; Dachsel, H.; Deegan, M.; Dyall, K.; Elwood, D.; Glendening, E.; Gutowski, M.; Hess, A.; Jaffe, J.; Johnson, B.; Ju, J.; Kobayashi, R.; Kutteh, R.; Lin, Z.; Littlefield, R.; Long, X.; Meng, B.; Nakajima, T.; Niu, S.; Pollack, L.; Rosing, M.; Sandrone, G.; Stave, M.; Taylor, H.; Thomas, G.; Lenthe, J. v.; Wong, A.;

Zhang, Z. *NWChem, A Computational Chemistry Package for Parallel Computers*, version 4.5 ed.; Pacific Northwest National Laboratory: Richland, Washington 99352, 2003.

(43) Frisch, M. J.; Trucks, G. W.; Schlegel, H. B.; Scuseria, G. E.; Robb, M. A.; Cheeseman, J. R.; Montgomery, J. A., Jr.; Vreven, T.; Kudin, K. N.; Burant, J. C.; Millam, J. M.; Iyengar, S. S.; Tomasi, J.; Barone, V.; Mennucci, B.; Cossi, M.; Scalmani, G.; Rega, N.; Petersson, G. A.; Nakatsuji, H.; Hada, M.; Ehara, M.; Toyota, K.; Fukuda, R.; Hasegawa, J.; Ishida, M.; Nakajima, T.; Honda, Y.; Kitao, O.; Nakai, H.; Klene, M.; Li, X.; Knox, J. E.; Hratchian, H. P.; Cross, J. B.; Bakken, V.; Adamo, C.; Jaramillo, J.; Gomperts, R.; Stratmann, R. E.; Yazyev, O.; Austin, A. J.; Cammi, R.; Pomelli, C.; Ochterski, J. W.; Ayala, P. Y.; Morokuma, K.; Voth, G. A.; Salvador, P.; Dannenberg, J. J.; Zakrzewski, V. G.; Dapprich, S.; Daniels, A. D.; Strain, M. C.; Farkas, O.; Malick, D. K.; Rabuck, A. D.; Raghavachari, K.; Foresman, J. B.; Ortiz, J. V.; Cui, Q.; Baboul, A. G.; Clifford, S.; Cioslowski, J.; Stefanov, B. B.; Liu, G.; Liashenko, A.; Piskorz, P.; Komaromi, I.; Martin, R. L.; Fox, D. J.; Keith, T.; Al-Laham, M. A.; Peng, C. Y.; Nanayakkara, A.; Challacombe, M.; Gill, P. M. W.; Johnson, B.; Chen, W.; Wong, M. W.; Gonzalez, C.; Pople, J. A. *Gaussian 03*, revision B.02; Pittsburgh, PA, 2003.

(44) Montgomery, J. A., Jr.; Frisch, M. J.; Ochterski, J. W.; Petersson, G. A. *J. Chem. Phys.* **1999**, *110*, 2822.

(45) Boys, S. F.; Bernardi, R. *Mol. Phys.* **1970**, *19*, 553.

(46) van Duijneveldt, F. B.; van Duijneveldt de Rijdt, J. G. C. M.; van Lenthe, J. H. *Chem. Rev.* **1994**, *94*, 1873.

(47) Feller, D.; Glendening, E. D.; Woon, M. W.; Feyereisen, J. *J. Chem. Phys.* **1995**, *103*, 3526.

(48) Feller, D. *Chem. Phys. Lett.* **2000**, *322*, 543.

(49) Hoyau, S.; Norrman, K.; McMahon, T. B.; Ohanessian, G. *J. Am. Chem. Soc.* **1999**, *121*, 8864.

(50) McMahon, T. B.; Ohanessian, G. *Chem.—Eur. J.* **2000**, *6*, 2931.

(51) Armentrout, P. B.; Rodgers, M. T. *J. Phys. Chem. A* **2000**, *104*, 2238.

(52) Wong, C. H. S.; Siu, F. M.; Ma, N. L.; Tsang, C. W. *THEOCHEM* **2002**, *588*, 9.

(53) Lee, S.-W.; Kim, H. S.; Beauchamp, J. L. *J. Am. Chem. Soc.* **1998**, *120*, 3188.

(54) Menozzi, A.; Appiani, G. *Gazz. Chim. Ital.* **1892**, *22*, 105.

(55) Blomback, B. *Methods Enzymol.* **1967**, *11*, 398.

(56) Ye, S. J.; Moision, R. M.; Armentrout, P. B. *Int. J. Mass Spectrom.* **2005**, *240*, 233.

(57) Amicangelo, J. C.; Armentrout, P. B. *Int. J. Mass Spectrom.* **2001**, *212*, 301.

(58) Amicangelo, J. C.; Armentrout, P. B. *J. Phys. Chem. A* **2004**, *108*, 10698.

(59) Rodgers, M. T.; Armentrout, P. B. *Mass Spectrom. Rev.* **2000**, *19*, 215.